Flexural performance of FRP reinforced concrete elements

Ilker Fatih Kara[a,b *] and Ashraf F. Ashour[b]

[a] Civil Engineering Department, Nigde University, Nigde, Turkey

[b] School of Engineering, Design and Technology, University of Bradford, BD7 1DP, UK

Abstract

A numerical method for estimating the curvature, deflection and moment capacity of FRP reinforced concrete beams is developed. Force equilibrium and strain compatibility equations for a beam section divided into a number of segments are numerically solved due to the non-linear behaviour of concrete. The deflection is then obtained from the flexural rigidity at mid-span section using the deflection formaule for various load cases. A proposed modification to the mid-span flexural rigidity is also introduced to account for the experimentally observed wide cracks over the intermediate support of continuous FRP reinforced concrete beams.

Comparisons with experimental results show that the proposed numerical technique can accurately predict moment capacity, curvature and deflection of FRP reinforced concrete beams. The ACI-440.1R-06 equations reasonably predicted the moment capacity of FRP reinforced concrete beams but progressively underestimated the deflection of continuous ones. On the other hand, the proposed modified formula including a correction factor for the beam flexural rigidity reasonably predicted deflections of continuous FRP reinforced concrete beams. It was also shown that a large increase in FRP reinforcement slightly increases the moment capacity of FRP over-reinforced concrete beams but greatly reduces the defection after first cracking.

Keywords: Concrete, deflection, moment capacity, effective moment of inertia, Fibre reinforced polymer

* Corresponding author; Email: ifkara@nigde.edu.tr

1. Introduction

Many reinforced concrete structures in severe environment are susceptile to steel corrosion and structural decay resulting in costly repair and service inconvenience. In order to avoid such problems, the use of fiber-reinforced polymer (FRP) bars as internal longitudinal flexural reinforcement has emerged as an alternative solution. In addition to their noncorrosive nature, FRP bars have a high strength-to-weight ratio making them attractive as reinforcement for concrete structures.

FRP reinforced concrete members behave differently from these reinforced with traditional steel. FRP bars have higher strength, but lower modulus of elasticity than steel, and exhibit linear stress–strain response up to failure. The lower modulus of elasticity of FRP causes a substantial decrease in the stiffness of FRP reinforced concrete beams after cracking and consequently higher levels of deflections under service conditions. Hence, the design of FRP reinforced concrete members is typically governed by serviceability requirements and analytical methods for predicting the service load deflections of FRP reinforced concrete members with a reasonable degree of accuracy would be very benefical. In addition, FRP reinforced concrete members exhibit poor structural ductility owing to the non ductile characteristics of FRP reinforcement and concrete, and, therefore an accurate prediction of their moment capacity is essential to avoid such brittle failure.

Over the last two decades, a number of studies have been carried out to investigate the flexural response of FRP reinforced concrete beams [1-21]. In the case of serviceability, and specifically for deflection calculations, several researchers have proposed empirical modifications to Branson's equation used in steel design codes [3, 7, 9, 11], while others have proposed a modified equivalent moment of inertia obtained from curvatures [22, 23]. On the other hand, concrete crushing flexural failure mode is generally preferred to FRP tensile

rupture, since it is more progressive and leads to a less catastrophic failure with a higher degree of deformability [24-26].

Razaqpur et al. [27] proposed an analytical model for computing the deflection of FRP reinforced concrete beams based on an assumed tri-linear variation for the moment-curvature response. In their model, the deflections of FRP reinforced concrete beams were computed assuming the entire beam to be fully cracked, followed by an adjustment for uncracked regions. However, the tension stiffening effect is ignored in this approach. In another investigation, Gravina and Smith [28] developed an analytical method to analyze the flexural behavior of statically indeterminate concrete beams reinforced with FRP bars. Their approach is able to model the progressive formation of flexural cracks and their spacings, and was found to be highly dependent on the input parameters such as the bond characteristics of FRP bars and surrounding concrete.

In the present study, a numercal technique has been developed to predict the moment-curavature relationship and hence moment capacity of FRP reinforced concrete beams. In the proposed procedure, a sectional analysis is carried out where the cross-section of FRP reinforced concrete member is divided into a number of concrete segment. The member deflection is then calculated from the moment-curvature relationship. The present study has also evaluated the ACI 440.1R-06 [24] equations for moment capacity and deflection against the experimental results of continuously and simply supported FRP reinforced concrete beams.

2. Constitutive Laws of Materials

Figure 1 gives the stress-strain relationships of concrete and FRP reinforcement implemented in this investigation. However, the numerical technique proposed can accommodate other

material models. The concrete stress-strain model in compression shown in Fig. 1(a) is adopted for its simplicity and computational efficiency. It can be written as [29]:

$$f_c = f_c' \left(\frac{2\varepsilon_c}{\varepsilon_{co}} - \left(\frac{\varepsilon_c}{\varepsilon_{co}} \right)^2 \right) \qquad \varepsilon_c < \varepsilon_{cu} \qquad (1)$$

where f_c and ε_c are the compressive stress and strain in concrete, respectively, $f_c^{'}$ is the cylinder compressive strength of concrete, ε_{co} $(= 2f_c^{'}/E_c)$ is the strain in concrete at maximum stress, where E_c is the initial tangent modulus of concrete and ε_{cu} (*=0.0035*) is the ultimate strain of concrete as shown in Figure 1(a).

A bi-linear stress-strain relationship is adopted to model concrete in tension as shown in Fig. 1(b) and given below:

$$f_t = E_t \varepsilon_t \qquad \varepsilon_t \le \varepsilon_{ct} \qquad (2(a))$$

$$f_t = f_{tu} - \frac{f_{tu}}{\mu \varepsilon_{ct}} (\varepsilon_t - \varepsilon_{ct}) \qquad \varepsilon_{ct}(1+\mu) \ge \varepsilon_t > \varepsilon_{ct} \qquad (2(b))$$

where f_t and ε_t are the tensile stress and strain in concrete, respectively, f_{tu} $(=0.62\sqrt{f_c^{'}})$ and ε_{ct} are the tensile strength and corresponding tensile strain of concrete, respectively, E_t is the tensile modulus of concrete, assumed to be the same as E_c, and μ is a factor controlling the rate of tensile strength decay. The tension stiffening effect is represented in the above model to account for concrete between cracks as it has a significant effect on member stiffness.

The stress-strain relationship of FRP bars is linear elastic up to rupture and given by:

$$f_f = E_f \varepsilon_f \qquad \varepsilon_f \le \varepsilon_{fu} \qquad (3)$$

where f_f and ε_f are the stress and strain in FRP bars, respectively, E_f is the modulus of elasticity of FRP bars, and f_{fu} and ε_{fu} are the ultimate strength and strain of FRP bars, respectively, as shown in Figure 1(c).

3. Moment-curvature relationship of FRP reinforced concrete sections

Figure 2 presents a concrete section reinforced with top and bottom FRP bars, that is divided into a number of segments, *n*. The numerical analysis starts by assuming a small value of strain at the concrete extreme compression fiber (or tensile FRP bars). For each strain ε_c at the top level of concrete section (or strain ε_f in tensile FRP bars), the neutral axis depth, *x*, is initially assumed and the correct value is iteratively obtained when equilibrium of forces is satisfied. According to the assumption that plane section before bending remains plane after bending, the strain in each concrete segment is linearly proportional to its distance from the neutral axis (Figure 2(b)) as expressed below:

$$\varepsilon_i = \frac{x - x_i}{x}\varepsilon_c \tag{4}$$

where ε_c is the strain at the top compression level of the reinforced concrete section and ε_i is the concrete compressive or tensile strain at mid-depth of *i*-th segment.

Assuming perfect bond between concrete and FRP bars, strains in tensile and compressive FRP bars can also be obtained from:

$$\varepsilon_f{}' = \frac{x - d'}{x}\varepsilon_c \tag{5}$$

$$\varepsilon_f = \frac{x - d}{x}\varepsilon_c \tag{6}$$

where ε_f and ε_f' indicate the strains in bottom and top FRP bars, respectively, and d and d' are the bottom and top FRP reinforcement depths, respectively.

The corresponding stresses in each concrete segment, and tensile and compressive reinforcements can be calculated from the respective stress-strain relationships of concrete and FRP presented in Fig. 1. The total concrete force including the contribution of compressive and tensile forces is calculated using Eqs. (7) below:

$$F_c = \sum_{i=1}^{n} f_{ci} h_i b \quad (7)$$

where f_{ci} is the concrete compressive or tensile stress at the centroid of the i th segment, h_i (=h/n) is the thickness of the i th segment and b is the beam width. This summation extends over all compressive and tensile segments of concrete section. The forces in top and bottom FRP bars are estimated from:

$$T_f = A_f E_f \varepsilon_f \quad (8)$$

$$C_f = A_f^{'} E_f^{'} \varepsilon_f^{'} \quad (9)$$

where T_f, A_f, and E_f are the force, area, and modulus of elasticity of bottom FRP bars, respectively, whereas C_f, $A_f^{'}$ and $E_f^{'}$ are the corresponding values of top FRP reinforcement. Eqs. (8) and (9) are valid for different types of FRP bars, i.e., GFRP, AFRP and CFRP, provided that the appropriate modulus of elasticity, E_f, and tensile rupture, f_{fu}, are used. The current analysis is also developed for steel compression reinforcement. In such case, the modulus of elasticity and yield strength of compression steel reinforcement are used in calculating the force C_f . Considering the equilibrium of forces, the following equation is obtained:

$$F_c + C_f = T_f$$

$$\sum_{i=1}^{n} f_{ci} h_i b + A_f^{'} E_f^{'} \varepsilon_f^{'} = A_f E_f \varepsilon_f \quad (10)$$

In the above Eq. (10), the neutral axis depth x is in fact the only unknown. The value of x is iteratively adjusted using the bi-section method and the procedure is repeated until sufficient equilibrium accuracy is attained as given below:

$$\frac{\left|F_c + T_f + C_f\right|}{\left|F_c\right|} \le 10^{-8} \tag{11}$$

The curvature φ of the member can also be determined from the strain distribution as follows (see Fig. 2(b)):

$$\varphi = \frac{\varepsilon_c}{x} \tag{12}$$

The applied moment M_f of the section is then calculated by taking moments of internal forces about any horizontal axis; for instance about the neutral axis

$$M_f = \sum_{i=1}^{n} F_{ci}(x - x_i) + T_f(x - d) + C_f(x - d') \tag{13}$$

where F_{ci} ($=f_{ci}h_ib$) is the concrete compressive or tensile force at the centroid of the i-th segment.

The strain in the concrete extreme compression fibre of the section (or tensile FRP bars) is incrementally increased and the above procedure is iteratively repeated for each value of strain. The analysis is terminated when either the tensile strain in the bottom FRP reinforcement reaches the tensile rupture strain of FRP bars ($\varepsilon_f = \varepsilon_{fu}$) or the concrete strain ε_c in the extreme compression fibre reaches the ultimate compressive strain ε_{cu} of concrete (concrete crushing). The section moment capacity M_{fu} is, therefore, the highest moment attained by the section for various incremental strain values at the extreme compression concrete fibre or bottom FRP bars.

Based on the aforementioned procedure, a computer program has been developed for the section moment capacity and moment-curvature relationship of FRP reinforced concrete elements.

4 Validation of the numerical technique against experimental results

4.1 *Flexural Moment Capacity*

Test results of 107 FRP reinforced concrete beams are collected from previous experimental investigations in the literature [1-21] and used to validate the proposed numerical method. Table 1 lists the geometrical and material properties of all beams considered. All the 107 beams were reported to have failed in flexure; either by concrete crushing or FRP rupture failure modes.

In addition to the developed numerical technique, the ACI 440 equations for moment capacity will also be compared against the experimental results in the database collected. The ACI 440.1R-06 report, based on the balanced FRP reinforcement ratio ρ_{fb} obtained from Eq. (14) below, predicted the moment capacity M_{fu} of beams reinforced with FRP bars using Eqs. 15 and 16 when the reinforcement ratio ρ_f is greater than ρ_{fb}, and by applying Eqs. 17 and 18 when the reinforcement ratio ρ_f is less than ρ_{fb}.

$$\rho_{fb} = 0.85\beta_1 \frac{f_c'}{f_{fu}} \frac{E_f \varepsilon_{cu}}{E_f \varepsilon_{cu} + f_{fu}} \tag{14}$$

$$M_{fu} = \rho_f f_f \left(1 - 0.59 \frac{\rho_f f_f}{f_c'}\right) bd^2 \tag{15}$$

$$f_f = \sqrt{\frac{(E_f \varepsilon_{cu})^2}{4} + \frac{0.85\beta_1 f_c'}{\rho_f} E_f \varepsilon_{cu}} - 0.5 E_f \varepsilon_{cu} \le f_{fu} \tag{16}$$

$$M_{fu} = A_f f_{fu} \left(d - \frac{\beta_1 c_b}{2}\right) \tag{17}$$

$$c_b = \left(\frac{\varepsilon_{cu}}{\varepsilon_{cu} + \varepsilon_{fu}}\right) d \tag{18}$$

where ρ_f (=A_f /*bd)* is the FRP reinforcement ratio, A_f is the area of tensile FRP reinforcement, f_f is the FRP stress at which concrete crushing failure mode occurs, c_b is the neutral axis depth for balanced failure as defined by Eq. 18, and β_1 is a strength reduction factor taken as 0.85 for concrete strength up to and including 27.6 MPa. For strength above 27.6 MPa, the factor β_1 is reduced continuously at a rate of 0.05 for every 6.9 MPa of strength in excess of 27.6 MPa, but is not taken less than 0.65.

Table 1 and Figure 3 compare the predictions from the current numerical analysis and ACI 440 (Eqs. (14) to (18)) against the experimental moment capacities of 107 FRP reinforced concrete beams in the database collected. The average and standard deviation of the ratio between the present technique and experimental bending capacities are 1.01 and 15%, respectively, whereas the corresponding values between ACI predictions and experimental moment capacities are 0.91% and 17%, respectively. The predictions obtained from the current analysis and ACI 440 are in very good agreement with the experimental results. The ACI 440.1R-06 equations have mostly underestimated the load capacity of FRP reinforced concrete beams. This may be attributed to the fact that the ACI 440 equation ignores the reinforcement in the compression zone. The tensile rupture and concrete crushing failure modes are correctly predicted by the the persent technique for 92% of beams considered (98 beams) as indicated in Table 1.

4.1.1 Effect of amount of FRP reinforcement on bending capacity

The present procedure has been employed to study the effect of increasing the area of FRP bars, represented by the FRP reinforcement ratio ρ_f*(=100As/bd)*, on the normalised flexural moment capacity $\mu(=M_{fu}/bd^2)$ as shown in Fig. 4: Fig. 4(a) for GFRP reinforcment and Fig. 4(b) for CFRP reinforcement. These two figures are produced for three different concrete compressive strengths $f_c^{'}$, namely $f_c^{'}$ = 30, 40 and 50 N/mm^2 and typical mechanical

properties of GFRP and CFRP as given in Fig. 4. The transition from under-reinforced to over-reinforced case is identified and marked on each curve. While the concrete compressive strength has no effect on the normalised flexural moment capacity μ of under-reinforced sections, it has a significant influence for over-reinforced case. For the under-reinforced sections, the normalised moment capacity μ is linearly proportional to the FRP reinforcement ratio ρ_f. On the other hand, a large increase in FRP reinforcement ratio ρ_f produces a little increase in the normalised moment capacity μ for the over-reinforced case.

4.2 Moment-curvature relationship

In this section, the moment-curvature results obtained from the numerical technique are compared with the experimental results of B4 and B9 FRP reinforced concrete simply supported beams tested by Thiagarajan [21] and presented in Fig. 5. Geometrical dimensions, reinforcement details and material properties of B4 and B9 FRP reinforced concrete beams considered are given in Table 2. The numerical results are in good agreement with the moment-curvature test results for the applied loads up to failure. The same figure also indicates that the proposed technique is able to predict the bending stiffness before and after cracking up to the complete failure of the beams considered.

4.3 Prediction of deflection

In the current numerical procedure, the flexural rigidity, EI_{eff}, of the member at the location of the maximum moment is firstly determined from the moment-curvature relationship at each loading as in Eq. 19 below:

$$EI_{eff} = \frac{M}{\varphi} \tag{19}$$

The midspan deflection, Δ, of FRP reinforced concrete beams is then calculated using the elastic deflection formula, for example; the immediate deflection of simply supported beams loaded with two- point loads, each *P/2*, could be calculated from Eq. 20 below:

$$\Delta = \frac{(P/2)(3L^2 - 4a^2)}{24EI_{eff}} \tag{20}$$

where a is the shear span and *L* is the span length or the mid-span deflection of continuously supported beams loaded with a mid-span point load, *P*, could be also computed from equation (21) as follows:

$$\Delta = \frac{7}{768}\frac{(PL^3)}{EI_{eff}} \tag{21}$$

In addition to the developed numerical technique, the ACI 440 equations for deflection calculations will be compared against the experimental results and the developed numerical technique. The ACI Committee 440 [24] provides a modified version of Branson's equation that includes a reduction coefficient, β_d, related to the reduced tension stiffening exhibited by FRP-reinforced concrete members as follows:

$$I_{eff} = \left(\frac{M_{cr}}{M}\right)^3 \beta_d I_1 + \left[1 - \left(\frac{M_{cr}}{M}\right)^3\right] I_2 \tag{22}$$

$$\beta_d = 0.2\left(\frac{\rho_f}{\rho_{fb}}\right) \tag{23}$$

where M_{cr} is the flexural cracking moment, M is the applied bending moment, β_d is a reduction coefficient, I_1 is the gross moment of inertia and I_2 is the moment of inertia of transformed cracked section.

In the present study the deflection of several FRP reinforced concrete beams experimentally tested elsewhere have been calculated by using the numerical procedure presented above. However, for the sake of brevity, only few examples covering simply and continuously supported beams are presented below.

4.3.1 Simply supported FRP reinforced concrete beams

The mid-span experimental deflections of C1-4, C2-4, G1-6 and G1-8 FRP reinforced concrete simply supported beams tested by Kassem et al. [4] are compared with the predictions from the numerical technique and ACI 440; see Fig. 6. Geometrical dimensions, reinforcement details and material properties of FRP reinforced concrete beams considered are given in Table 2. All beams were subjected to two symmetrical point loads and reinforced with various types and amounts of FRP bottom longitudinal reinforcement. The deflections results obtained from the present numerical technique and ACI 440 are in good agreement with the test results for the applied loads up to failure. However, the numerical technique gives a better prediction of deflections than the ACI model. Fig. 6 also indicates that the present technique is able to predict both the pre and post cracking deflections up to beam failure.

A sensitivity analysis has also been conducted to investigate the effect of FRP reinforcement type and amount on the mid-span deflection of FRP reinforced concrete beams as presented below.

4.3.1.1 Effect of amount of FRP on beam deflections

The influence of tensile reinforcement ratio (ρ_f) on mid-span deflection of FRP reinforced concrete beams as predicted by the current method is presented in Fig. 7: Fig. 7(a) for C1-4, C1-6 and C1-8 concrete beams reinforced with CFRP and Fig. 7(b) for G1-6 and G1-8

concrete beams reinforced with GFRP. The geometrical dimensions, reinforcement and material details of the beams considered are given in Table 2, indicating that the only parameter changed was the amount of tensile FRP reinforcement whereas other parameters were the same for beams shown in each figure. It can be observed that increasing the tensile reinforcement ratio greatly reduces the defection after first cracking, for example the tensile reinforcement ratio of beam C1-8, which was twice as that of beam C1-4, has a significant effect on the reduction of deflection of this beam in comparison to that of beam C1-4.

4.3.1.2 Effect of type of FRP on beam deflections

The deflection of a set of beams having geometrical and mechanical properties similar to those of beams tested by Kassem et al. [4] have been calculated for different types of FRP reinforcement. Fig. 8 presents the moment-deflection relationships of these beams with different types of FRP bars. Fig. 8 indicates that beams reinforced with GFRP bars exhibit a significant reduction in stiffness after the initiation of first crack in comparison with these reinforced with CFRP reinforcement. This behaviour is attributed to the low elastic modulus of GFRP bars compared with that of CFRP bars; that affects the ability of these bars to control concrete cracks, leading to a reduced effective moment of inertia and hence large deflections.

4.3.2 Continuously supported FRP reinforced concrete beams

Further verification of the proposed technique has been conducted by comparison with the results of GcUO, GcOO, GS1 and C-C-3 continuous FRP reinforced concrete beams [19, 20, 30]. Each continuous beam consisted of two equal spans, was loaded by a single point load at the middle of each span and was reinforced with either GFRP or CFRP bars. Geometrical dimensions, reinforcement details and materials properties of continuous beams considered are given in Table 2. Since the measured displacements at the middle of each span were

similar [19, 20, 30], one side mid-span displacement is compared against the predictions obtained from the numerical technique for continuous beams.

In the above experimental investigations [19, 20, 30], it was observed that wide cracks occurred over the intermediate support of continuous reinforced concrete beams; consequently ACI or present numerical analysis may underestimate the deflection of such members. So in addition to the numerical technique presented above, a modified flexural rigidity, EI_{eff}, at the cracked mid-span section including a reduction coefficient, α, has been proposed for the statically indeterminate concrete beams reinforced with FRP bars as below:

$$\mathrm{EI}_{\mathrm{eff}} = (EI)_2 \frac{\alpha}{\left(1 - 0.5(1-\alpha)\left(\frac{\mathrm{M}_{\mathrm{cr}}}{\mathrm{M}}\right)\right)} \tag{24a}$$

$$\alpha = 0.65\left[0.7 + 0.36\left(\frac{E_f}{E_s}\right)\left(\frac{\rho_f}{\rho_{fb}}\right)\right] \le 0.65 \qquad \text{for GFRP or AFRP beams} \tag{24b}$$

$$\alpha = 0.65\left[0.7 + 0.12\left(\frac{E_f}{E_s}\right)\left(\frac{\rho_f}{\rho_{fb}}\right)\right] \le 0.65 \qquad \text{for CFRP beams} \tag{24c}$$

Fig. 9 provides the comparison between experimental and theoretical results of the load versus mid-span deflection response of continuous FRP reinforced concrete beams considered. It can be seen from the figure that the numerical method and ACI model underestimate the deflections of the continuous beams at loads higher than the cracking load. As the load is increased, this underestimation is progressively increased until the end of loading. Such discrepancies could be referred to the occurrence of wide cracks over the middle support of continuous beams as reported in [19, 20, 30]. However, the proposed modified equation (24) which includes the reduction factor α to calculate the effective flexural rigidity of continuous FRP reinforced concrete beams gives a better prediction of deflections for all continuous beams considered.

5. Conclusions

An iterative numerical method for predicting the flexural behaviour of FRP reinforced concrete beams has been presented. The moment-curvature relationship of FRP reinforced concrete beams is numerically obtained by considering force equilibrium and strain compatibility. The beam deflection is then calculated from the mid-span curvature.

Comparisons between the predicted deflections and curvatures of FRP reinforced concrete beams and experimental results available in the literature show good agreement. In addition, the predicted moment capacities of 107 FRP reinforced concrete beams are in very good agreement with experimental results. While the ACI model gives reasonable predictions of simply supported FRP reinforced concrete beam deflections, it progressively underestimates deflections of continuous FRP reinforced concrete beams. However, the proposed modified formula including a correction factor for the flexural rigidity gives a closer deflection to experimental results of FRP reinforced concrete continuous beams.

A parametric study concluded that concrete compressive strength has no effect on the moment capacity of FRP under-reinforced concrete beams but a significant influence for over-reinforced ones. On the other hand, a large increase in FRP reinforcement slightly increases the moment capacity of FRP over-reinforced concrete beams but greatly reduces the defection after first cracking.

ACKNOWLEDGMENT

The first author acknowledges the financial support of the Higher Education Council (YOK) of Turkey.

References

[1] AlMusallam TH, Al-Salloum YA, Alsayed SH, Amjad MA. Behavior of concrete beams doubly reinforced by FRP bars. In: Proceedings of the third international symposium on non-metallic (FRP) reinforcement for concrete structures (FRPRCS-3), Japan, vol. 2; 1997. p. 471–478.

[2] The´riault M, Benmokrane B. Effects of FRP reinforcement ratio and concrete strength on flexural behavior of concrete beams. J Compos Constr 1998;2(1):7–16.

[3] Toutanji HA, Saafi M. Flexural behavior of concrete beams reinforced with glass fiber-reinforced polymer (GFRP) bars. ACI Struct J 2000;97(5):712–9.

[4] Kassem C, Farghaly AS, Benmokrane B. Evaluation of flexural behavior and serviceability performance of concrete beams reinforced with FRP Bars. J Compos Constr 2011; doi:10.1061/(ASCE)CC.1943-5614.0000216 .

[5] Benmokrane B, Chaallal O, Masmoudi R. Glass fibre reinforced plastic (GFRP) rebars for concrete structures. Constr Build Mater 1995;9(6):353–364.

[6] Ashour AF. Flexural and shear capacities of concrete beams reinforced with GFPR bars. Constr Build Mater 2006;20:1005–15.

[7] Benmokrane B, Chaallal O, Masmoudi R. Flexural response of concrete beams reinforced with FRP reinforcing bars. ACI Struct J 1996;91(2):46–55.

[8] Yost JR, Goodspeed CH, Schmeckpeper ER. Flexural performance of concrete beams reinforced with FRP grids. J Compos Constr 2001;5(1):18–25.

[9] Masmoudi R, The´riault M, Benmokrane B. Flexural behavior of concrete beams reinforced with deformed fiber reinforced plastic reinforcing rods. ACI Struct J 1998;95(6):665–76.

[10] Alsayed SH. Flexural behaviour of concrete beams reinforced with GFRP bars. Cem Concr Compos 1998;20(1):1–11.

[11] Brown VL, Bartholomew CL. FRP reinforcing bars in reinforced concrete members. ACI Mater J 1993;90(1):34–9.

[12] Grace NF, Soliman AK, Abdel-Sayed G, Saleh KR. Behavior and ductility of simple and continuous FRP reinforced beams. J Compos Constr 1998;2(4):186–94.

[13] Duranovic N, Pilakoutas K, Waldron P. Tests on concrete beams reinforced with galss fibre reinforced plastic bars. In: Proceedings of the third international symposium on non-metallic (FRP) reinforcement for concrete structures (FRPRCS 3), Japan, vol. 2; 1997. p. 479–86.

[14] Pecce M, Manfredi G, Cosenza E. Experimental response and code models of GFRP RC beams in bending. J Compos Constr 2000;4(4):182–90.

[15] Ashour AF, Family M. Tests of concrete flanged beams reinforced with CFRP bars. Magazine of Concrete Research 2006, 58(9): 627-639.

[16] Rafi MM, Nadjai A, Ali F, Talamona D. Aspects of behaviour of CFRP reinforced concrete beams in bending. Constr Build Mater 2008;22:277-285.

[17] Alsayed SH, Al-Salloum YA, Almusallam TH. Performance of glass fiber reinforced plastic bars as a reinforcing material for concrete structures. Compos Part 2000; 31: 555-567.

[18] Barris C, Torres LI, Turon A, Baena M, Catalan A. An experimental study of the flexural behaviour of GFRP RC beams and comparison with prediction models. Compos Struct; 2009; 91: 286-295.

[19] Ashour AF, Habeeb MN. Continuous concrete beams reinforced with CFRP bars, Struct Build 2008; SB6: 349-357.

[20] Mostafa EM, Amr ER, Ehab ES. Flexural behavior of continuous FRP reinforced concrete beams, J Compos Constr, 2010; 14(6): 669–680.

[21] Thiagarajan G. Experimental and analytical behavior of carbon fiber-based rods as flexural reinforcement. J Compos Constr, 2003; 7(1): 64-72.

[22] Faza SS, Ganga Rao HVS. Pre- and post-cracking deflection behaviour of concrete beams reinforced with fiber-reinforced plastic rebars. In: Neale KW, Labossiere P, editors. Proceedings of the first international conference on the use of advanced composite materials in bridges and structures (ACMBS I). Montreal: Canadian Society for Civil Engineering; 1992. p. 151–60.

[23] Bischoff PH. Reevaluation of deflection prediction for concrete beams reinforced with steel and fiber-reinforced polymer bars. J Struct Eng 2005; 131(5): 752–767.

[24] ACI Committee 440. Guide for the design and construction of concrete reinforced with FRP Bars (ACI 440.1R-06), Farmington Hills, Michigan (USA): American Concrete Institute; 2006.

[25] CSA Standard CAN/CSA-S806-02. Design and construction of building components with fiber-reinforced polymers. Mississauga, Ontario, Canada: Canadian Standards Association; 2002.

[26] Razaqpur AG, Isgor OB. Methods for calculating deflections of FRP reinforced concrete structures. In: Proceeding of the 3rd International Conference on Advanced Composite Materials in Bridges and Structures, August 2000; Ottawa, Canada, 2000; 371–378.

[27] Razaqpur AG, Svecova D, Cheung MS. Rational method for calculating deflection of fiber reinforced polymer reinforced beams. ACI Struct J, 2000; 97(1): 175–84.

[28] Gravina RJ, Smith, ST. Flexural behaviour of indeterminate concrete beams reinforced with FRP bars. Eng Struct, 2008; 30(9): 2370–2380.

[29] Hsu, TTC. Unified theory of reinforced concrete, Taylor & Francis Inc, 1992, 313p.

[30] Habeeb MN, Ashour AF, Flexural behavior of continuous GFRP reinforced concrete beams, J Compos Constr, 2008; 12(1): 115–124.

FIGURE CAPTIONS

Fig. 1 FRP and concrete stress–strain relationships.

Fig. 2 Strains, stresses and forces of concrete section reinforced with FRP bars.

Fig. 3 Experimental versus predicted moment capacities of FRP reinforced concrete beams

Fig. 4. Effect of increasing the area of FRP bars on the flexural moment capacity

Fig. 5 Comparison of predicted and experimental moment-curvature relationships of simply supported FRP reinforced concrete beams

Fig. 6 Comparison between experimental and predicted deflections of simply supported FRP beams.

Fig. 7 Effect of tensile reinforcement ratio on deflections of FRP reinforced concrete beams

Fig. 8 Effect of different types of FRP on the midspan deflections of FRP reinforced beams

Fig. 9 Comparison between experimental and predicted deflections of continuously supported FRP beams.

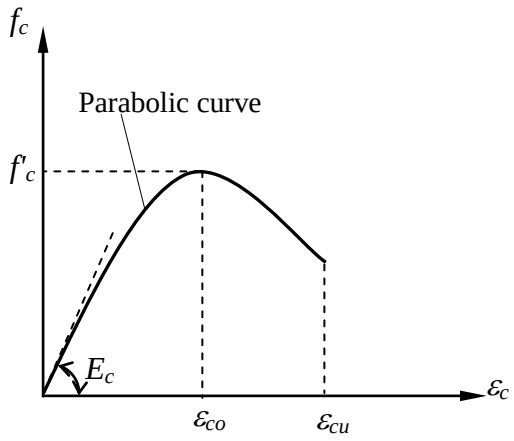

(a) Concrete in compression

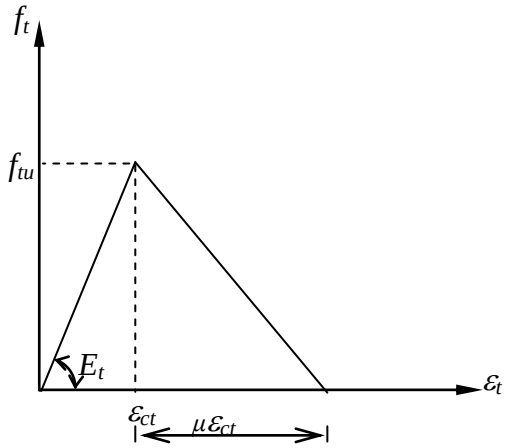

(b) Concrete in tension

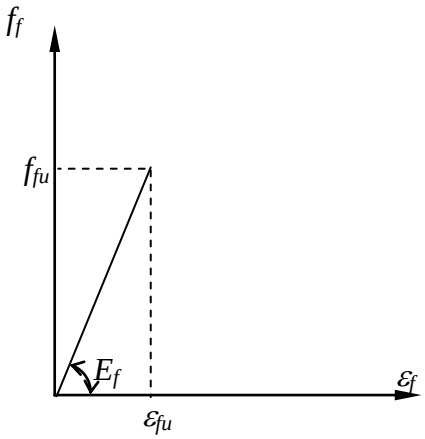

(c) FRP composites

Fig. 1 FRP and concrete stress–strain relationships.

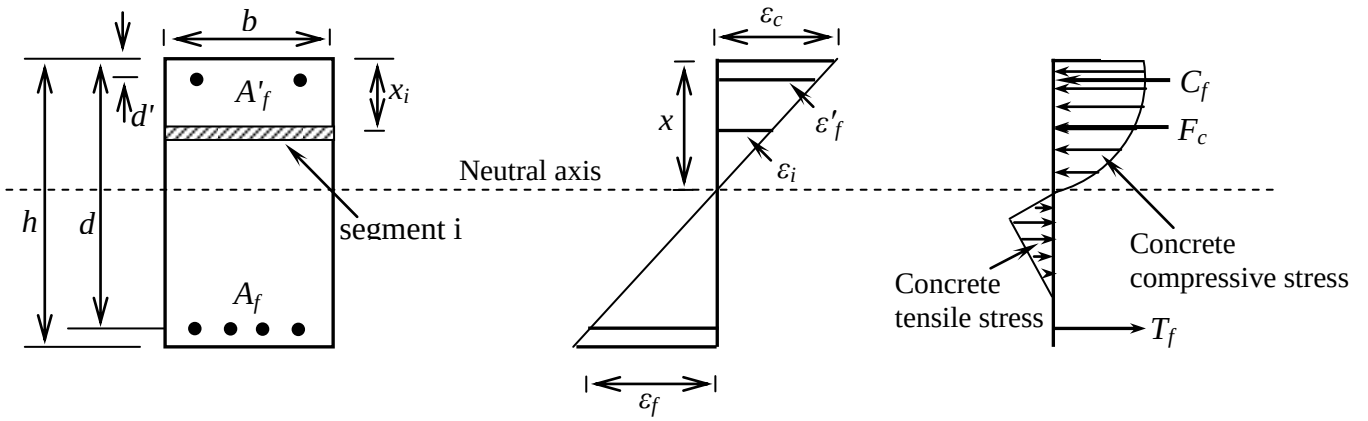

(a) FRP reinforced concrete section (b) Strain distribution (c) Stress distribution and forces

Fig. 2 Strains, stresses and forces of concrete section reinforced with FRP bars

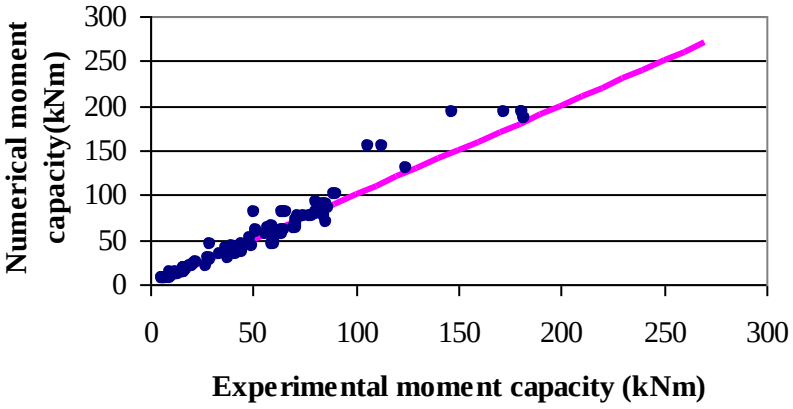

(a) Numerical technique

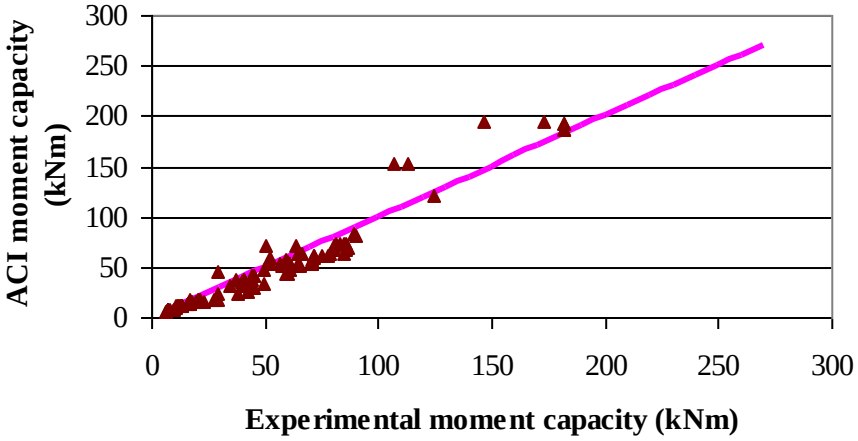

(b) ACI 440

Fig. 3 Experimental versus predicted moment capacities of FRP reinforced concrete beams

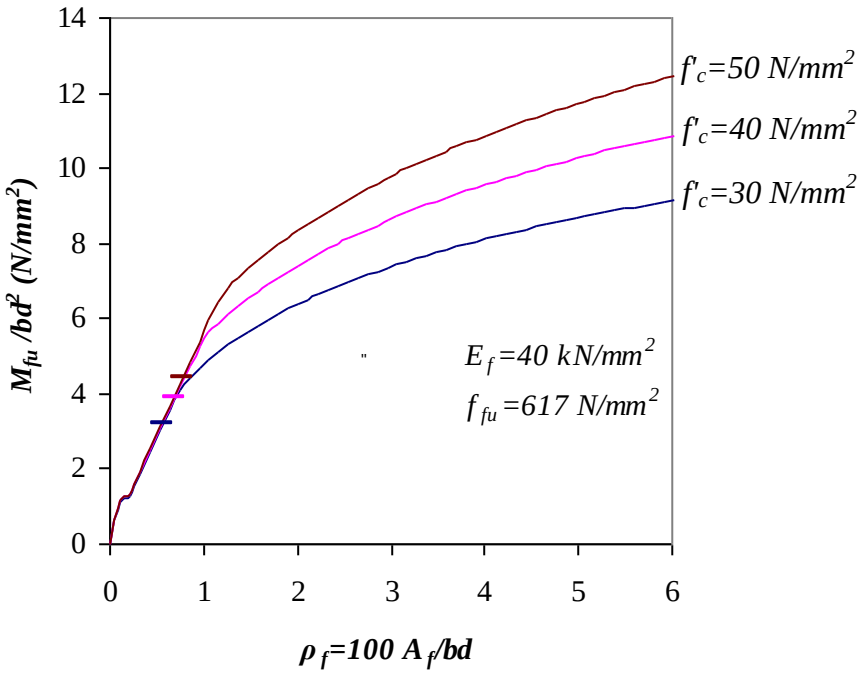

(a) GFRP reinforcement

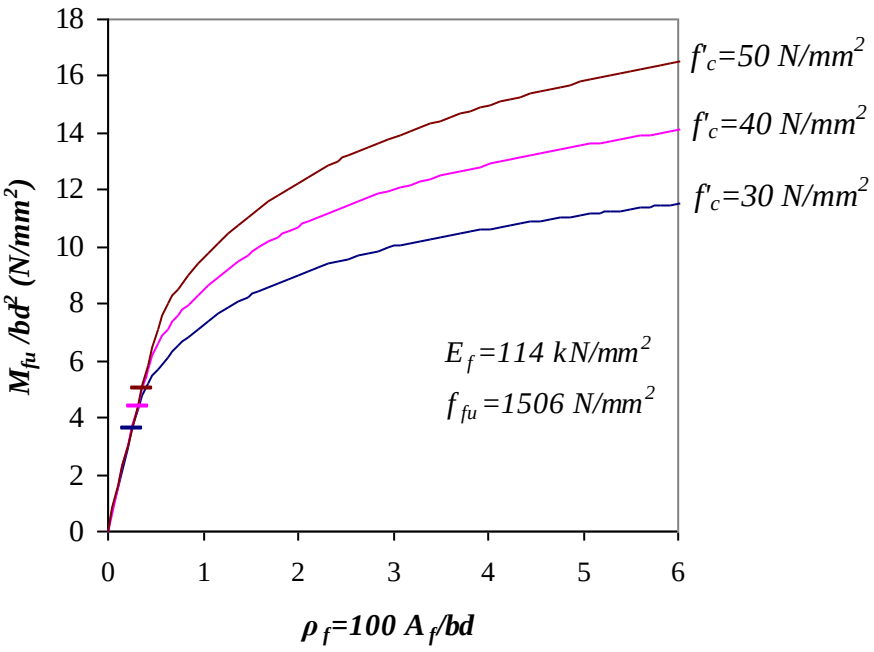

(b) CFRP reinforcement

Fig. 4 Effect of increasing the area of FRP bars on the flexural moment capacity.

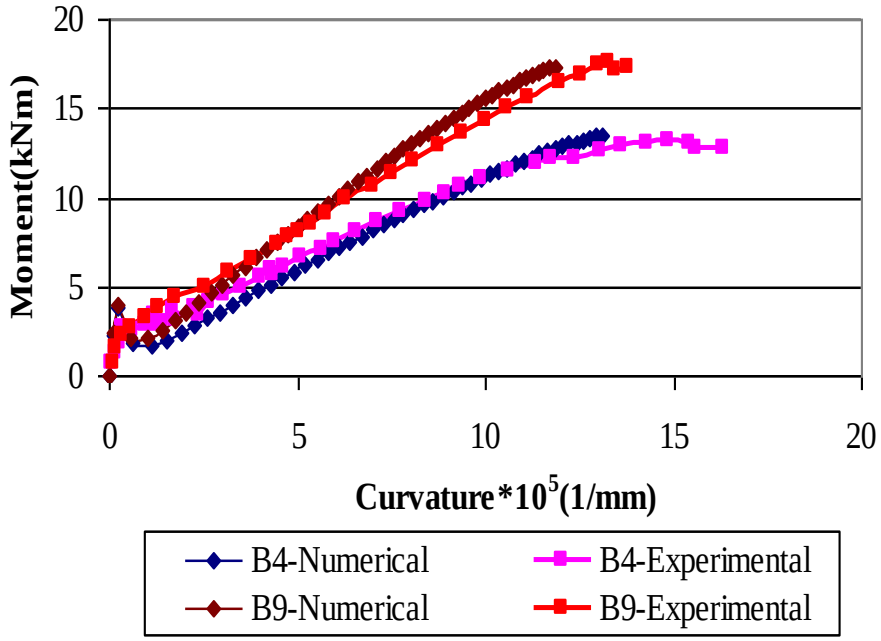

Fig. 5 Comparison of predicted and experimental moment-curvature relationships of simply supported beams

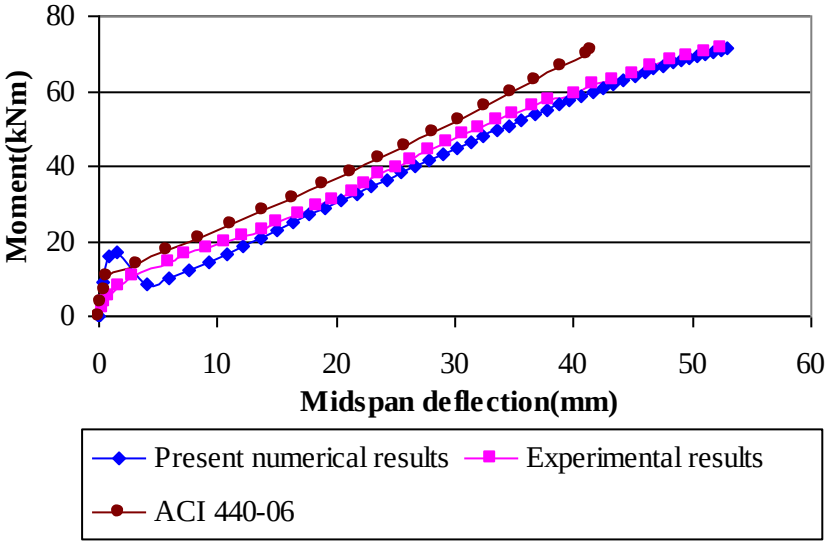

(a) Beam C1-4

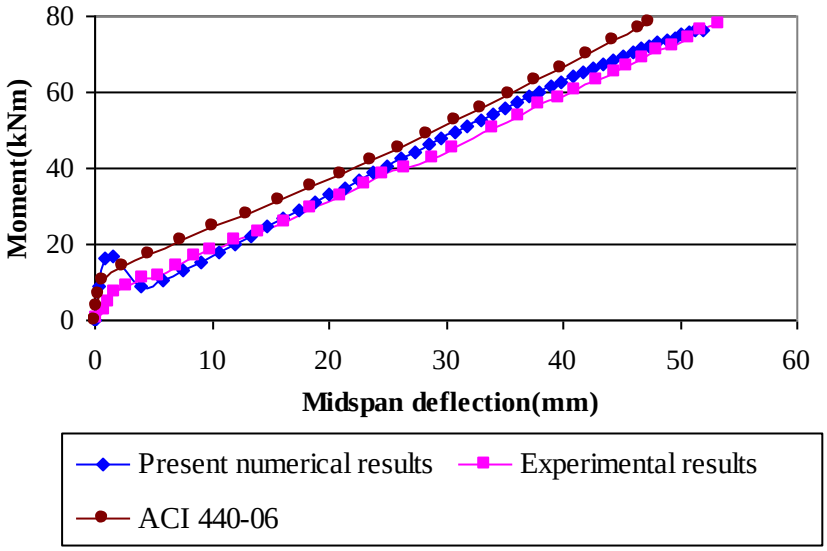

(b) Beam C2-4

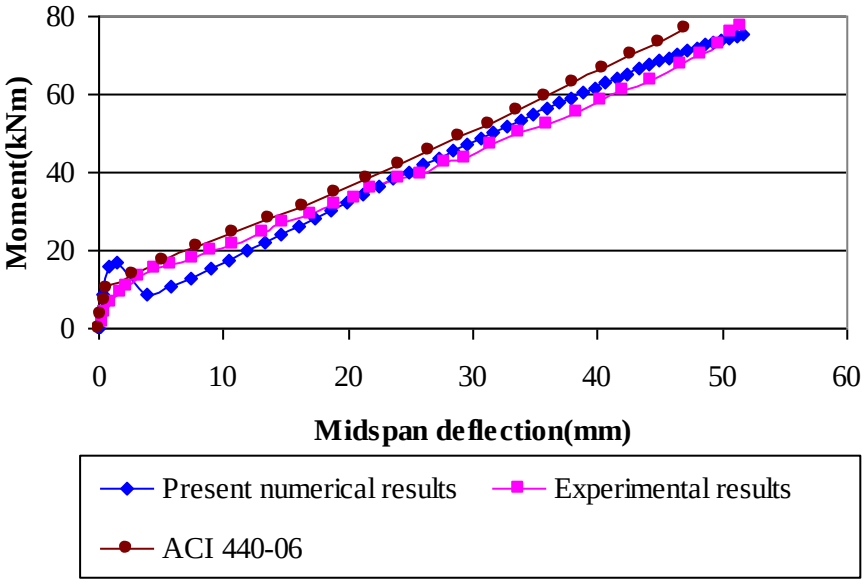

(c) Beam G1-6

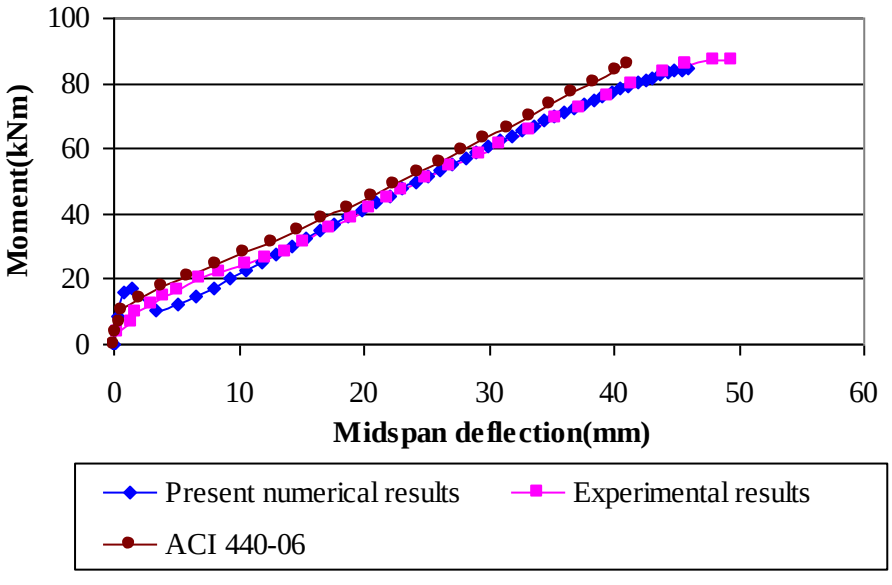

(d) Beam G1-8

Fig. 6 Comparison between experimental and predicted deflections of simply supported FRP beams.

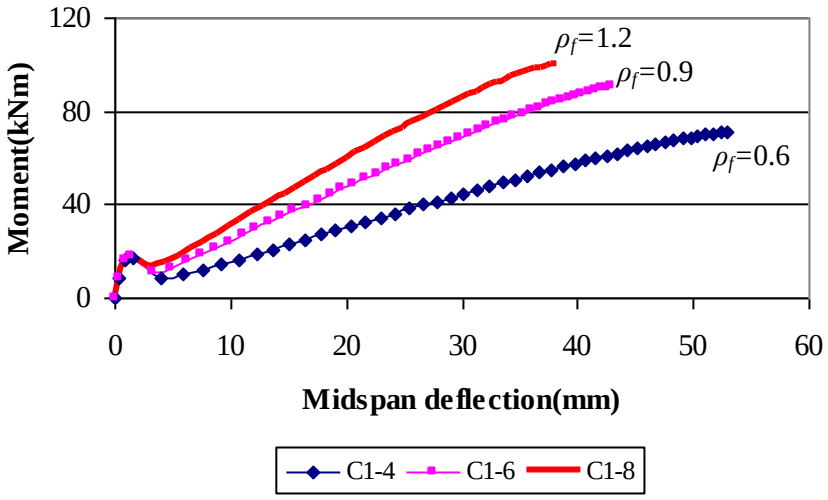

(a) CFRP bars

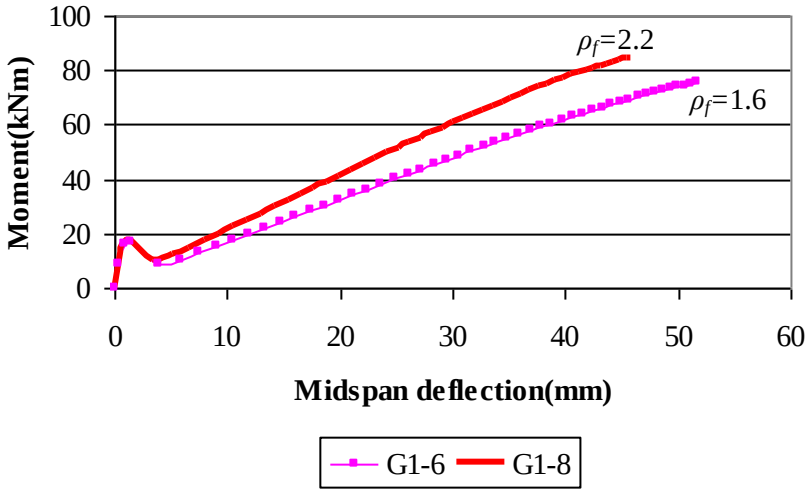

(b) GFRP bars

Fig.7 Effect of tensile reinforcement ratio on deflections of FRP reinforced concrete beams

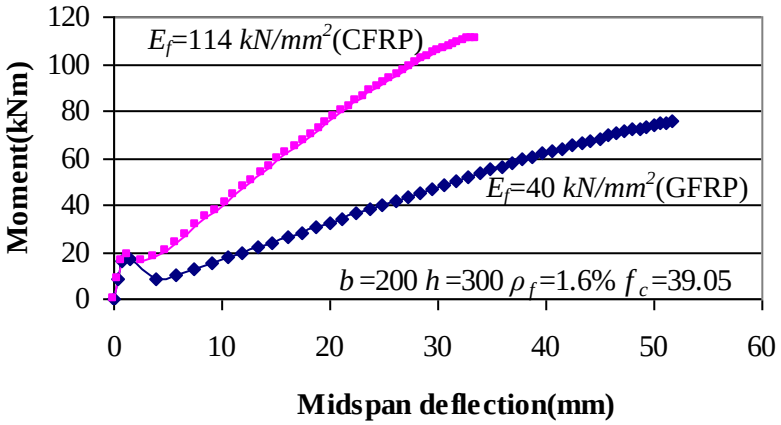

Fig. 8 Effect of different types of FRP on the midspan deflections of FRP reinforced beams

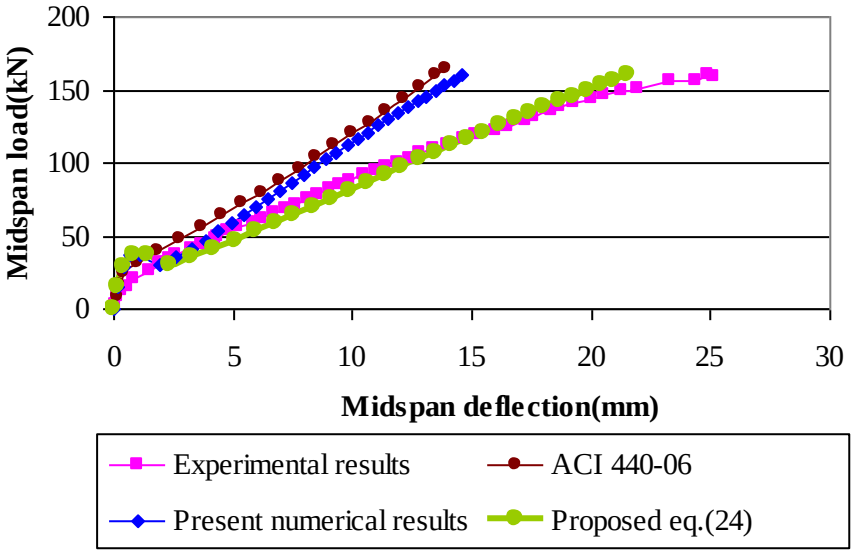

(a) Beam GcUO

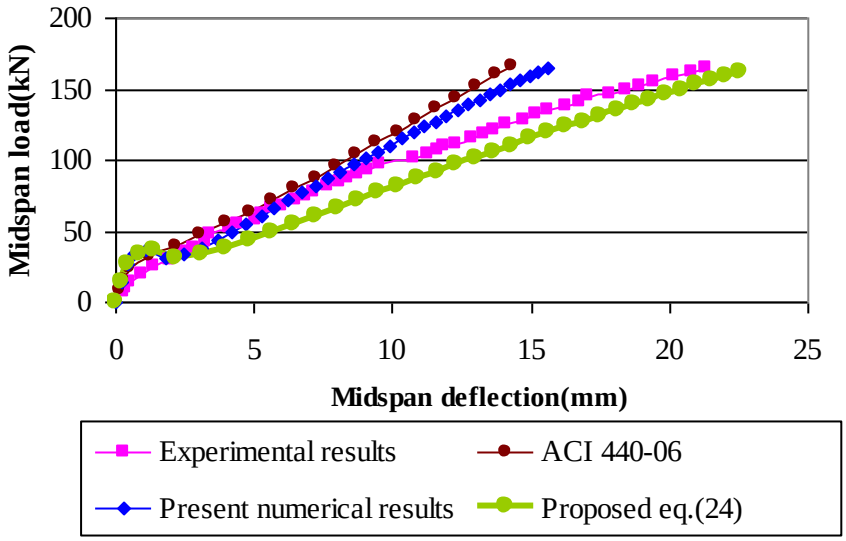

(b) Beam GcOO

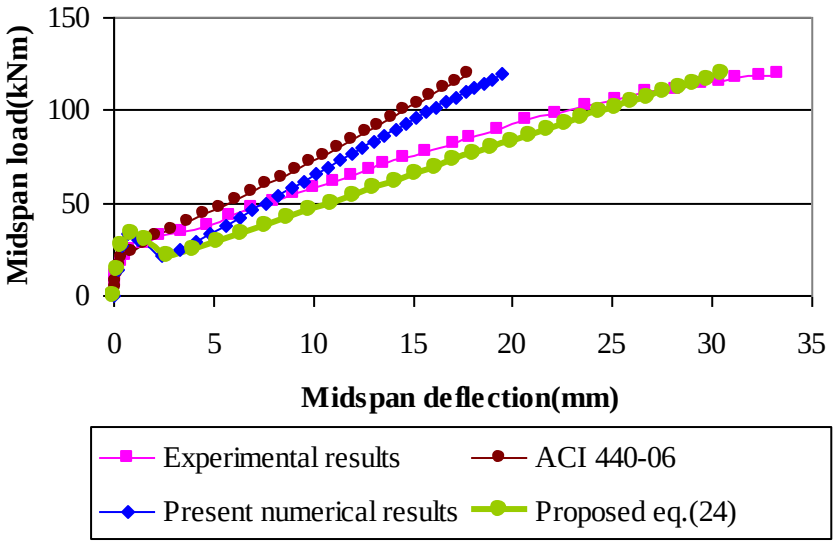

(c) Beam GS1

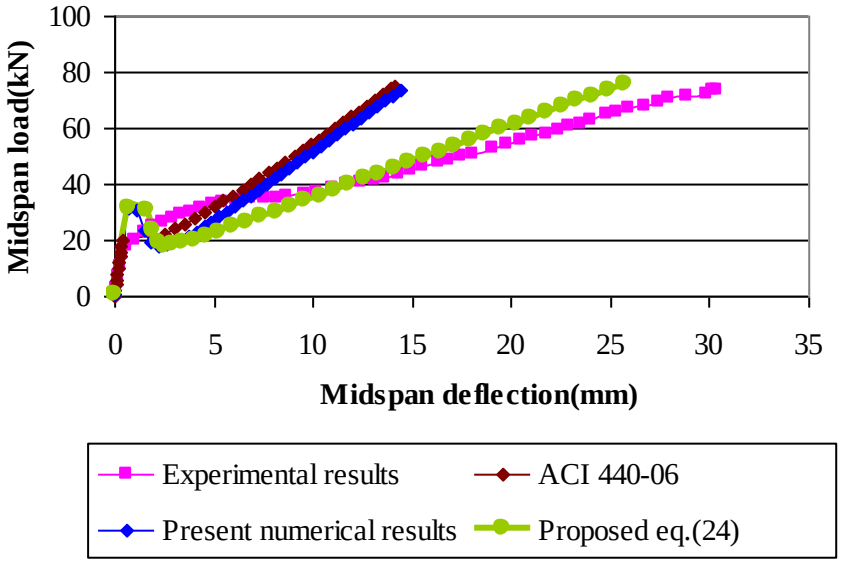

(d) Beam CC3

Fig. 9 Comparison between experimental and predicted deflections of continuously supported FRP beams.

TABLE CAPTIONS

Table 1 Comparisons between the theoretical and experimental flexural capacities.

Table 2 Details of simply and continuously supported FRP reinforced concrete beams used in the numerical technique validation.

Table 1 Comparisons between the theoretical and experimental flexural capacities.

Reference	Beam notation	Width (mm)	Overall depth (mm)	f_c' (MPa)	ρ_f (%)	M_{exp} (kN)	M_{fu}/M_{exp}		Experimental mode of failure
							Current technique	ACI 440 [24]	
[1]	COMP-00	200	240	35.4	1.33	40.25	1.01	0.92	Concrete Crushing
	COMP-25	200	240	36.4	1.33	40.25	1.02	0.93	Concrete Crushing
	COMP-50	200	240	36.5	1.33	40.25	1.03	0.93	Concrete Crushing
	COMP-75	200	240	37.5	1.33	44.28	0.96	0.86	Concrete Crushing
[2]	BC2HA	130	180	57.2	1.24	19.7	0.98	0.80	Concrete Crushing
	BC2HB	130	180	57.2	1.24	20.6	0.94	0.77	Concrete Crushing
	BC2VA	130	180	97.4	1.24	22.7	1.12	0.69	Concrete Crushing[c]
	BC4NB	130	180	46.2	2.7	20.6	0.97	0.82	Concrete Crushing
	BC4HA	130	180	53.9	2.7	21	1.04	0.85	Concrete Crushing
	BC4HB	130	180	53.9	2.7	21.4	1.02	0.83	Concrete Crushing
	BC4VA	130	180	93.5	2.7	28.4	1.05	0.65	Concrete Crushing
	BC4VB	130	180	93.5	2.7	29.5	1.01	0.62	Concrete Crushing
[3]	GB1-1	180	300	35	0.53	60	0.73	0.72	Concrete Crushing[c]
	GB1-2	180	300	35	0.53	59	0.74	0.73	Concrete Crushing[c]
	GB2-1	180	300	35	0.79	65	0.94	0.79	Concrete Crushing
	GB2-2	180	300	35	0.79	64.3	0.95	0.80	Concrete Crushing
	GB3-1	180	300	35	1.1	71	0.90	0.75	Concrete Crushing
	GB3-2	180	300	35	1.1	70.5	0.90	0.76	Concrete Crushing
[4]	C1-4	200	300	40.4	0.6	71.2	1.00	0.83	Concrete Crushing
	C1-6	200	300	39.3	0.9	83.13	1.09	0.89	Concrete Crushing

Table 1 (continued)

Reference	Beam notation	Width (mm)	Overall depth (mm)	f_c' (MPa)	ρ_f (%)	M_{exp} (kN)	M_{fu}/M_{exp}		Experimental mode of failure
							Current technique	ACI 440 [24]	
[4]	C1-8	200	300	39.3	1.2	90.39	1.11	0.91	Concrete Crushing
	C2-4	200	300	39.9	0.5	78.75	0.97	0.80	Concrete Crushing
	C2-6	200	300	40.8	0.8	80.89	1.13	0.92	Concrete Crushing
	C2-8	200	300	40.8	1.1	89.39	1.13	0.92	Concrete Crushing
	G1-6	200	300	39.05	1.6	77.47	0.97	0.81	Concrete Crushing
	G1-8	200	300	39.05	2.2	86.76	0.98	0.80	Concrete Crushing
	G2-6	200	300	39.05	1.4	71	0.96	0.80	Concrete Crushing
	G2-8	200	300	39.05	1.9	84.54	0.91	0.75	Concrete Crushing
	AR-6	200	300	39.05	0.9	70.85	0.92	0.77	Concrete Crushing
	AR-8	200	300	39.05	1.2	71.75	1.03	0.86	Concrete Crushing
[5]	ISO30-2	200	300	42	1.06	80.4	1.01	0.90	Concrete Crushing
	KD30-1	200	300	42	1.06	50.6	1.60	1.41	Concrete Crushing
	KD30-2	200	300	42	1.06	63.8	1.27	1.12	Concrete Crushing
	KD45-1	200	450	52	0.68	106.6	1.45	1.44	Concrete Crushing[c]
	KD45-2	200	450	52	0.68	113	1.37	1.36	Concrete Crushing[c]
	ISO55-1	200	550	42	0.55	181.5	1.06	1.07	FRP rupture
	ISO55-2	200	550	42	0.55	181.5	1.06	1.07	FRP rupture
	KD55-1	200	550	42	0.55	146.9	1.31	1.32	FRP rupture
	KD55-2	200	550	42	0.55	172.5	1.11	1.12	FRP rupture
[6]	Beam2	150	200	27.68	0.23	5.886	0.99	0.97	FRP rupture
	Beam4	150	250	27.68	0.17	7.848	0.97	0.95	FRP rupture
	Beam6	150	300	27.68	0.14	10.791	0.90	0.85	FRP rupture

Table 1 (continued)

Reference	Beam notation	Width (mm)	Overall depth (mm)	f_c' (MPa)	ρ_f (%)	M_{exp} (kN)	M_{fu}/M_{exp}		Experimental mode of failure
							Current technique	ACI 440 [24]	
[6]	beam8	150	200	50.09	0.23	5.886	1.00	0.99	FRP rupture
	beam10	150	250	50.09	0.17	9.483	0.81	0.80	FRP rupture
	beam12	150	300	50.09	0.14	16.75	1.12	1.11	FRP rupture
[7]	ISO2	200	300	43	1.13	80.4	0.96	0.84	Concrete Crushing
	ISO3	200	550	43	0.57	181.7	1.02	1.03	FRP rupture
	ISO4	200	550	43	0.57	181.7	1.02	1.03	FRP rupture
[8]	1FRP1	381	203	27.6	0.12	11.49	0.99	0.98	FRP rupture
	1FRP2	381	203	27.6	0.12	12.67	0.90	0.89	FRP rupture
	1FRP3	381	203	27.6	0.12	11.49	0.99	0.98	FRP rupture
	2FRP1	318	216	27.6	0.13	13.62	0.90	0.88	FRP rupture
	2FRP2	318	216	27.6	0.13	13.26	0.92	0.91	FRP rupture
	2FRP3	318	216	27.6	0.13	13.06	0.93	0.92	FRP rupture
	4FRP1	203	152	27.6	1.27	15.78	0.91	0.86	Concrete Crushing
	4FRP2	203	152	27.6	1.27	15.58	0.92	0.88	Concrete Crushing
	4FRP3	203	152	27.6	1.27	16.29	0.88	0.84	Concrete Crushing
	5FRP1	191	152	27.6	1.35	16.37	0.84	0.80	Concrete Crushing
	5FRP2	191	152	27.6	1.35	16.65	0.83	0.79	Concrete Crushing
	5FRP3	191	152	27.6	1.35	15.78	0.87	0.83	Concrete Crushing
[9]	CB2B-1	200	300	52	0.69	57.9	1.09	0.93	Concrete Crushing[c]
	CB2B-2	200	300	52	0.69	59.8	1.05	0.90	Concrete Crushing[c]
	CB3B-1	200	300	52	1.04	66	1.22	0.97	Concrete Crushing
	CB3B-2	200	300	52	1.04	64.8	1.24	0.99	Concrete Crushing

Table 1 (continued)

Reference	Beam notation	Width (mm)	Overall depth (mm)	f_c' (MPa)	ρ_f (%)	M_{exp} (kN)	M_{fu}/M_{exp}		Experimental mode of failure
							Current technique	ACI 440 [24]	
[9]	CB4B-1	200	300	45	1.47	75.4	1.01	0.83	Concrete Crushing
	CB4B-2	200	300	45	1.47	71.7	1.07	0.87	Concrete Crushing
	CB6B-1	200	300	45	2.2	84.8	1.06	0.86	Concrete Crushing
	CB6B-2	200	300	45	2.2	85.4	1.06	0.86	Concrete Crushing
[11]	1	152	152	35.9	0.38	7.04	1.02	0.99	FRP rupture
	2	152	152	36.9	0.38	6.64	1.09	1.06	FRP rupture
	4	152	152	38.9	0.38	7.23	1.00	1.00	FRP rupture
	5	152	152	39.9	0.38	7.35	0.99	0.99	FRP rupture
	6	152	152	40.9	0.38	6.75	1.07	1.09	FRP rupture
[12]	cb-st	152	350	48.26	0.23	51.91	1.18	1.15	FRP rupture
[13]	GB5	150	250	31.2	1.36	40.3	0.86	0.81	Concrete Crushing
	GB9	150	250	39.8	1.36	39.73	1.02	0.91	Concrete Crushing
	GB10	150	250	39.8	1.36	39.5	1.02	0.92	Concrete Crushing
[14]	F2	500	185	30	0.7	36.8	1.08	1.03	Concrete Crushing
	F3	500	185	30	1.22	60.7	0.83	0.78	Concrete Crushing
[15]	RC2	200	350	34.43	0.36	85.27	0.81	0.78	FRP rupture
	RC4	200	350	34.43	0.72	124.6	1.05	0.98	Concrete Crushing[c]
[16]	BRC2	120	200	41.71	0.7	29.19	0.95	0.78	Concrete Crushing
[17]	II	200	210	31.3	3.6	34.1875	0.99	0.93	Concrete Crushing
	III	200	260	31.3	1.2	45.125	0.97	0.91	Concrete Crushing
	IV	200	300	40.7	1.15	59.1875	1.09	0.97	Concrete Crushing
	V	200	250	40.7	2.87	57	1.03	0.92	Concrete Crushing

Table 1 (continued)

Reference	Beam notation	Width (mm)	Overall depth (mm)	f_c' (MPa)	ρ_f (%)	M_{exp} (kN)	M_{fu}/M_{exp}		Experimental mode of failure
							Current technique	ACI 440 [24]	
[18]	C-212-D1	140	190	59.8	0.99	38.22	0.79	0.62	Concrete Crushing
	C-216-D1	140	190	56.3	1.78	45.06	0.81	0.64	Concrete Crushing
	C-316-D1	140	190	55.2	2.67	49.38	0.84	0.67	Concrete Crushing
	C-212-D2	160	190	39.6	0.99	27.69	0.75	0.65	Concrete Crushing
	C-216-D2	160	190	61.7	1.78	42.15	0.78	0.61	Concrete Crushing
	C-316-D2	160	190	60.1	2.67	43.2	0.88	0.68	Concrete Crushing
[19]	C-S-1	200	300	26.9	0.42	64.11	0.88	0.84	FRP rupture
	C-S-2	200	300	27.5	0.16	44.28	0.97	0.95	FRP rupture
	C-C-3[a]	200	300	23.6	0.16	44.76	0.95	0.94	FRP rupture
	C-C-4[a]	200	300	27.2	0.42	60.66	0.93	0.89	FRP rupture
	C-C-5[a]	200	300	28	0.42	56.03	1.01	0.96	FRP rupture
[20]	CS1[a]	200	300	26	0.42	51.8	1.10	1.02	Concrete Crushing
	CS1[b]	200	300	26	0.28	29	1.55	1.56	Concrete Crushing[c]
	GS1[a]	200	300	28	1.18	60.2	1.02	0.94	Concrete Crushing
	GS1[b]	200	300	28	0.79	49	1.06	0.98	Concrete Crushing
[21]	B4	152.4	152.4	51.73	0.34	12.603	1.07	1.01	Concrete Crushing
	B5	152.4	152.4	48.02	0.34	10.151	1.28	1.22	FRP rupture
	B7	152.4	152.4	49.3	0.53	17.104	0.98	0.86	Concrete Crushing
	B8	152.4	152.4	51.1	0.53	16.919	1.01	0.88	FRP rupture

Table 1 (continued)

Reference	Beam notation	Width (mm)	Overall depth (mm)	f_c' (MPa)	ρ_f (%)	M_{exp} (kN)	M_{fu}/M_{exp}		Experimental mode of failure
							Current technique	ACI 440 [24]	
[21]	B12	152.4	152.4	43.88	0.76	17.506	1.08	0.92	FRP rupture
	B9	152.4	152.4	53.31	0.53	16.575	1.05	0.91	FRP rupture
Average							1.01	0.91	
Standart deviation (%)							0.15	0.17	

Note: f'_c is the compressive strength of concrete, ρ_f is the FRP reinforcement ratio (A_f/bd), M_{exp} is the experimental moment capacity and M_{fu} is the predicted moment capacity of FRP sections.

[a] Indicates the mid-span section of continuously supported FRP reinforced concrete beams.

[b] Indicates the middle support section of continuously supported FRP reinforced concrete beams.

[c] Indicates disagreement between predicted and experimentally observed flexural failure modes.

Table 2 Details of simply and continuously supported FRP reinforced concrete beams used in the numerical technique validation.

Reference	Beam notation	Supporting condition	Loading type	b (mm)	h (mm)	L(mm)	Reinforcing bars (mm)		E_f (kN/mm^2)	f'_c (N/mm^2)
							Top	Bottom		
[21]	B4	Simply supported	Two point	152.4	152.4	1524	2Φ12.7 (Steel)	2Φ6.35 (CFRP)	140	51.73
[21]	B9	Simply supported	Two point	152.4	152.4	1524	2Φ12.7 (Steel)	2Φ7.94 (CFRP)	140	53.31
[4]	C1-4	Simply supported	Two point	200	300	2750	2Φ11.3 (Steel)	4Φ9.5 (CFRP)	114	40.4
[4]	C1-6	Simply supported	Two point	200	300	2750	2Φ11.3 (Steel)	6Φ9.5 (CFRP)	114	39.3
[4]	C1-8	Simply supported	Two point	200	300	2750	2Φ11.3 (Steel)	8Φ9.5 (CFRP)	114	39.3
[4]	C2-4	Simply supported	Two point	200	300	2750	2Φ11.3 (Steel)	4Φ9 (CFRP)	122	39.9
[4]	G1-6	Simply supported	Two point	200	300	2750	2Φ11.3 (Steel)	6Φ12.7 (GFRP)	40	39.05
[4]	G1-8	Simply supported	Two point	200	300	2750	2Φ11.3 (Steel)	8Φ12.7 (GFRP)	40	39.05
[30]	GcUO	Continuously supported	Mid-span	200	300	2750	3Φ12.7 (GFRP)	6Φ15.9 (GFRP)	38.7(for Φ15.9) 44.2(for Φ12.7)	29
[30]	GcOO	Continuously supported	Mid-span	200	300	2750	6Φ15.9 (GFRP)	6Φ15.9 (GFRP)	38.7	25
[19]	C-C-3	Continuously supported	Mid-span	200	300	2750	2Φ12 (CFRP)	2Φ7.5 (CFRP)	200	23.6
[20]	GS1	Continuously supported	Mid-span	200	300	2800	2Φ16 (GFRP)	3Φ16 (GFRP)	46	28

Note: b, h and L = beam's width, depth and span, respectively, E_f is the modulus of elasticity of FRP longitudinal bars.